

used for the centrally placed Antenna 1 (layer-averaged SARs shown in Fig. 8a), calculations have been performed for Antennas 2 and 3 for the handset placed against both the right ear and against the left ear, respectively (see Figs. 8b and 8c). This was done since the transmitting elements of these antennas are asymmetrically placed on the chassis and, therefore, occupy slightly different positions vis à vis the head as the handset is placed against the right ear or the left ear, respectively. We therefore wanted to compare the SARs for both possible configurations. From Figs. 8b and 8c, it is interesting to note that the SARs are somewhat lower when the handset is held against the left ear. This is because the transmitting antenna (marked T in Figs. 6, 7) is somewhat further from the ear lobe, which is the region of the highest SARs. For an assumed input power of 0.6 W, the total power absorbed by the head for each of the antennas is given in Table 2. Also given in Table 2 are the values of the peak SARs for any 1 g of tissue (taken in the shape of a cube) and the values of the volume-averaged SARs for some of the important tissues. The powers absorbed by the head and neck, which are almost the same as for the whole body, are relatively small and well within safety guidelines [1]. The peak SARs for each of the configurations are also within the safety guidelines.

It is interesting to examine in detail the layer-averaged SAR distributions that are given in Figs. 8a, 8b, and 8c, respectively. As expected, the maximum layer-averaged SARs are for layers close to layer no. 69, which passes through the base of the driven antenna. From Fig. 8, the peak layer-averaged SARs (for layer no. 69) of 2.8, 33.9, and 6.5 mW/kg have been obtained for Antennas 1, 2, and 3, respectively. Also, the peak SARs averaged over any 1 g of tissue (defined as a tissue volume in the shape of a cube) are fairly small and occur generally for the upper part of the ear and the volume of the skin, skull, and brain immediately behind it. This region is close to the base of the driven elements of the various antennas. As given in Table 2, peak SARs for Antennas 1, 2, and 3 are calculated to be 0.25, 1.55, and 0.32 W/kg for the handsets held against the right ear, respectively. If the handset is on for about half the time of the required time-averaging

period of 15 minutes, the time-averaged peak SARs would be lower by a factor of 2 and would, therefore, always be less than 1 W/kg for any of the antennas that have been considered to date.

In Fig. 9 we show the calculated SAR distributions for three representative layers of the head for a radiated power of 0.6 W from Antenna 2 placed against the right side of the head. While layer no. 69 is in the xy plane containing the driving point of the antenna, layers 60 and 75 are 1.35 cm above and 0.9 cm below this plane, respectively. As expected, the SARs are highly superficial with the highest values for the region of the ear, the skin, and the surface of the brain. Very little energy is deposited for either the interior of the head or for the lower-conductivity skull.

VI. Experiments

A. Development of Tissue-Equivalent Materials

To develop the experimental model of the head, it was necessary to develop tissue-simulant materials for the brain, eyes, ears, muscle, and skull. For measurements of materials to simulate soft tissues (brain, eyes, muscle), we have used the open-ended coaxial line method that has been described in the literature [24, 25]. In this method the complex reflection coefficient Γ^* measured for the open end of the coaxial line can be used to calculate complex permittivity ϵ^* from the following equation:

$$\epsilon^* = \frac{1 - \Gamma^*}{j \omega Z_0 C_0 (1 + \Gamma^*)} - \frac{C_f}{C_0} \quad (4)$$

where Z_0 is the characteristic impedance (normally 50 Ω) for the coaxial line, C_0 is the capacitance when the line is in air, and C_f is the capacitance which accounts for the fringing fields in the dielectric of the coaxial line. We have used a nominal 3.6-mm Teflon-filled coaxial line ($a = 1.50$ mm, $b = 0.456$ mm) for which the following capacitances were

obtained using water (for which the dielectric properties are known) as the test medium:

$$C_0 = 0.022 \text{ pF}, C_T = C_0 + C_f = 0.027 \text{ pF}.$$

To calibrate the complex permittivity measurement system, a composition of 62.61% water, 0.5823% salt, 29.8% polyethylene powder, and 7.01% Superstuff* (a gelling agent) previously suggested by Guy et al. [26] was used for the initial set of measurements. For this composition, the measured dielectric properties have been given by these authors, albeit at a somewhat lower frequency of 2.45 GHz.

Using the network analyzer HP8510B, we measured the reflection coefficient Γ^* for the open end of the coaxial line that was embedded in this tissue-simulant material. Using Eq. 4, we obtained $\epsilon^* = 32.87 - j10.9$ at 2.45 GHz. This is in good agreement with the value of $\epsilon^* = 33.6 - j9.1$ given by Guy et al. [26] for this composition. For this same composition we have also measured ϵ^* at 6.0 GHz and find it to be $\epsilon^* = 33.0 - j12.71$.

The desired values of the dielectric constants and the conductivities for the various tissues have previously been given in Table 1. To arrive at the appropriate compositions, the following steps were taken for the various mixtures that have been tested.

1. For the first set of mixtures we used varying amounts of water (50, 60, 70, 80 and 90 percent), Superstuff* (7.0, 7.0, 7.0, 7.0 and 4.0 percent, respectively) and the polyethylene powder (43, 33, 23, 13, and 6 percent, respectively). Since water itself is quite lossy at 6.0 GHz, no salt was used for these initial compositions. Using the procedure described above, we obtained ϵ_r and σ for the various compositions that are plotted in Figs. 10a and 10b, respectively, as a function of the percentage water content of the mixtures. Several measurements were made for each of the mixtures and the data thus obtained are given in Figs. 10a and 10b. From the slopes of the measured values we can obtain the following factors

* A gelling agent TX151 supplied by Oil Center Research, P.O. Box 51871, LaFayette, LA, 70505.

$$K_{\sigma|_{H_2O}} = \frac{\Delta\sigma}{\Delta H_2O(\%)} = 0.04775 \quad (5)$$

$$K_{\epsilon_r|_{H_2O}} = \frac{\Delta\epsilon_r}{\Delta H_2O(\%)} = 0.801 \quad (6)$$

2. We next prepared a set of mixtures where the percentages of water and Superstuff were fixed at 70 percent and 7 percent, respectively while the salt (NaCl) content was varied to be 0.5, 1.0, 1.5, 2.0 and 2.5 percent, respectively. The fourth ingredient polyethylene powder was therefore varied to be 22.5, 22.0, 21.5, 21.0, and 20.5 percent, for the various mixtures. For these compositions the measured ϵ_r was relatively constant between 28 and 30, while σ increased with the percentage of the salt content as shown in Fig. 11. A factor $K_{\sigma|_{NaCl}}$ dependent on the salt content of the mixture could therefore be obtained from the results given in Fig. 11.

$$K_{\sigma|_{NaCl}} = \frac{\Delta\sigma}{\Delta NaCl(\%)} = 1.005 \quad (7)$$

From the measured slopes given by Eqs. 5-7 we could then estimate the compositions needed to simulate the various soft tissues namely brain, muscle, ears, and eyes, respectively. In Table 3 we give the needed complex dielectric properties ϵ_r and σ and the estimated compositions that were tested to simulate the various tissues. Also given in Table 3 are the measured values for the various compositions at 6 GHz. Since the measured values for the various selected compositions are close to the desired values, we used these

compositions to simulate the various soft tissues needed for the experimental model of the head and neck.

To simulate the skull, we started with a composition of 36.4 percent epoxy, 36.4 percent hardener, and the rest a potassium chloride (KCl) solution for which the KCl and water contents were 12 and 88 percent by weight, respectively. This composition had previously been used by Hartsgrrove et al. [27], albeit for frequencies up to 900 MHz. The method used for complex permittivity measurements was, however, slightly different, since it was not easy to make excellent gap-free contact for an open-ended coaxial probe with the hardened slabs that could be fabricated for this material. Instead, we used a short-circuited waveguide method described by Von Hippel [28]. In this method one measures the locations and the magnitudes of the minima in a short-circuited waveguide that is completely filled with a slab of the material placed against the short circuit. To get multiple measurements, we used several lengths of the materials of slightly altered compositions. The calculated values of ϵ_r and σ are given in Table 4. Since the measured values for the composition #2 with NaCl-based material are close to the desired values $\epsilon_r = 6.0$ and $\sigma = 0.3$ S/m for fat and bone (see Table 1), this composition was used to form the hollow mold in the form of the human head.

To create the hollow mold of skull-simulant material, the procedure was as follows. First of all, a mold of wood in the shape of the human head and neck was made. This mold was coated with layers of liquid rubber (Plasti Dip, made by PDI, Inc., Blaine, Minnesota) to form a thickness of 5-7 mm to correspond to the thickness of the desired hollow mold, which is in accordance with the thickness of the human skull. We next formed a Styrofoam block around the rubber-coated wooden mold for the right half of the mold. The layer of rubber was then cut around the central plane to remove the wooden mold and leave the layer of rubber sticking to the Styrofoam block corresponding to the right half of the model. The hollow corresponding to the right half of the model was then filled with wax for easier removal in subsequent steps. The layer of rubber sticking to the

Styrofoam block was next removed, leaving a gap of 5-7 mm between the mold of wax and the Styrofoam block. This gap was then filled with the saline-based epoxy composition described in Table 4 (composition #2). By removing the wax and Styrofoam molds after the epoxy had hardened, we could then obtain the right half of the model made of the skull-simulant material. Identical steps were then followed to create the left half of the model of the skull-simulant material. The hollow mold of the head and neck thus created was filled with the soft-tissue-simulant materials of Table 3, corresponding to brain, muscle, and eyes, with ears wrapped in Saran wrap attached to create a five-tissue experimental model that could then be used for experimental measurements.

B. Calibration of the Electric-Field Probe

As mentioned in Section I, the most sensitive technique for SAR measurements is to measure the internal electric fields (E) by an implantable E-field probe such as model BRH-15 [7] and calculate the SARs by using the relationship $SAR = \sigma E^2/\rho$. A miniature, broadband electric-field probe developed by Bassen and colleagues [7, 29] and marketed as Narda model 26089/BRH-15 probe, may be used for internal E-field measurements. This probe, described in references 7 and 29, uses three orthogonal pickup dipoles, each of length 2.5 mm with its own leadless diode detector operating in the square-law region. The sum of the three diode outputs obtained with an operational amplifier gives an output proportional to E^2 .

To calibrate the miniature E-field probe for use at 6 GHz, we have used both a slab model filled with tissue-simulant material and a rectangular waveguide WR 137 that was filled with a similar material. For the first arrangement the measured output voltage (generally microvolts) could be related to the values of E^2 that are obtained numerically using the FDTD method. Alternatively, for the rectangular waveguide, the probe output voltages measured for the lossy tissue-simulant filler medium may be compared with the electric fields that can be obtained using the analytical expressions.

C. Experimental SAR Distributions

For experimental determination of SAR distributions, we have used Antennas 1 and 2 placed against the right ear of the model. For the experimental model, the previously described skull-equivalent mold was filled with tissue-simulant materials representative of brain, muscle, eyes, and ears (Table 3).

Using the prototype Antennas 1 and 2 (see Figs. 5 and 6), measurements were made of the E-field distributions inside the experimental model using approximately 9 W of power available from an Avantek Model 64100 Amplifier. The SARs for the various locations were then calculated from the relationship $SAR = \sigma E^2/\rho$. The measured SAR variations for Antenna 2 inside the skull are given in Fig. 12 for different depths (y) for three different values of x (see the insert of Fig 12) corresponding to the edge of the chassis close to the transmitting antenna, and for the y axes corresponding to the center and the far edge of the chassis, respectively. For each of the three curves, the SARs were measured in the plane containing the driving point of the antenna. It is interesting to note in Fig. 12 that the local SARs in the brain-equivalent material are fairly small and considerably smaller than the safety guidelines. As expected, the SARs were even smaller for Antenna 1 (by about an order of magnitude) and have therefore not been plotted. We have also measured the maximum values of the SARs for both Antennas 1 and 2, respectively. The maximum SARs which invariably occurred for the ear are given in Table 5 and are compared with the SARs that were calculated from the numerical model. Agreement with the calculated values is quite good, both for Antenna 1 and Antenna 2, respectively. Even though the maximum local SAR for Antenna 2 is high, with the volume averaging for any 1 g of tissue (defined as a tissue volume in the shape of a cube), the volume-averaged SAR is considerably lower and is only 1.55 W/kg as given in Table 2.

VII. Comparison of the Data with the Safety Guidelines

Revised safety guidelines with respect to human exposure to radio frequency electromagnetic fields have recently been approved by IEEE and by ANSI [1]. According to these guidelines, an exposure condition is acceptable if it can be shown that SARs are below 0.08 W/kg, as averaged over the whole body, and spatial peak SAR values for any 1 g of tissue (defined as a tissue volume in the shape of a cube) is less than 1.6 W/kg. As seen in Table 2, the whole-body-averaged values for the three antennas considered for the handset are 0.06, 0.35, and 0.11 mW/kg, respectively, and are therefore orders of magnitude smaller than 0.08 W/kg or 80 mW/kg prescribed in the safety guidelines. Similarly, the peak SAR values averaged over any 1 g of tissue (defined as a tissue volume in the shape of a cube) are 0.25, 1.55, and 0.32 W/kg for the three proposed Antennas 1, 2, and 3, respectively. Whereas the peak SARs for Antennas 1 and 3 are clearly less than 1.6 W/kg prescribed in the RF safety guidelines of IEEE and ANSI, the peak SAR for Antenna 2 (1.55 W/kg) is close to the safety limit. However, as discussed in Section I, the SARs are to be averaged over a time duration of 15 minutes for an irradiation frequency of 6 GHz. If the handset is on for a fraction of the time for any 15-minute period, both the whole-body and peak SAR values given here would be proportionately less and hence well within the safety guidelines.

Acknowledgments

The authors gratefully acknowledge the contributions of Professor Mark Nielson and his students, Shane Dunleavy and Richard Maxwell, of the Department of Biology, University of Utah, in converting the MRI-based model to the electromagnetic model with identified tissues. This work was accomplished under the able supervision of Dr. James N. Lee of the Medical Imaging Laboratory, School of Medicine, University of Utah, using the computer software ANALYZE developed by the Mayo Clinic. Venkat Vallepalli assisted in the experimental work. His help in the experimental work is gratefully

acknowledged. The authors have also benefited from many helpful discussions with several colleagues at AT&T Bell Laboratories, in particular, Ron Petersen, Bala Krishnamurthy, John Seeman, Mark Vanderwalle, John Daly, and Joe DeAngelis.

REFERENCES

1. ANSI/IEEE C95.1-1992, "American National Standard -- Safety Levels with Respect to Human Exposure to Radio Frequency Electromagnetic Fields, 3 kHz to 300 GHz," published by the Institute of Electrical and Electronics Engineers, Inc., 345 East 47th Street, New York, New York, 10017.
2. O. P. Gandhi, "Numerical Methods for Specific Absorption Rate Calculations," Chapter 6, pp. 113-140, in *Biological Effects and Medical Applications of Electromagnetic Energy*, O. P. Gandhi, Editor, Prentice Hall, Inc., Englewood Cliffs, New Jersey, 1990.
3. I. Chatterjee, Y. G. Gu, and O. P. Gandhi, "Quantification of Electromagnetic Absorption in Humans from Body-Mounted Communication Transceivers," *IEEE Transactions on Vehicular Technology*, Vol. VT-34, pp. 55-62, 1985.
4. A. W. Guy and C. K. Chou, "Specific Absorption Rates of Energy in Man Models Exposed to Cellular UHF Mobile-Antenna Fields," *IEEE Transactions on Microwave Theory and Techniques*, Vol. MTT-34, pp. 671-680, 1986.
5. M. A. Stuchly, A. Kraszewski, S. S. Stuchly, G. W. Hartsgrrove, and R. J. Spiegel, "RF Energy Deposition in a Heterogeneous Model of Man: Near-Field Exposures," *IEEE Transactions on Biomedical Engineering*, Vol. BME-34, pp. 944-950, 1987.
6. R. F. Cleveland, Jr. and T. W. Athey, "Specific Absorption Rates in Models of the Human Head Exposed to Hand-Held UHF Portable Radios," *Bioelectromagnetics*, Vol. 10, pp. 173-186, 1989.
7. H. Bassen, M. Swicord, and J. Abita, "A Miniature Broadband Electric Field Probe," *Ann. New York Academy of Sciences*, Vol. 247, pp. 481-493, 1974.
8. D. M. Sullivan, O. P. Gandhi, and A. Taflove, "Use of the Finite-Difference Time-Domain Method in Calculating EM Absorption of Man Models," *IEEE Transactions on Biomedical Engineering*, Vol. BME-35, pp. 179-186, 1988.
9. J. Y. Chen and O. P. Gandhi, "RF Currents Induced in an Anatomically Based Model of a Human for Plane-Wave Exposures 20-100 MHz," *Health Physics*, Vol. 57, pp. 89-98, 1989.
10. K. S. Yee, "Numerical Solution of Initial Boundary Value Problems Involving Maxwell's Equations in Isotropic Media," *IEEE Transactions on Antennas and Propagation*, Vol. AP-14, pp. 302-307, 1966.
11. A. Taflove and M. E. Brodwin, "Computation of the Electromagnetic Fields and Induced Temperatures Within a Model of the Microwave Irradiated Human Eye," *IEEE Transactions on Microwave Theory and Techniques*, Vol. MTT-23, pp. 888-896, 1975.
12. A. Taflove and M. E. Brodwin, "Numerical Solution of Steady-State Electromagnetic Scattering Problems Using the Time-Dependent Maxwell's Equations," *IEEE Transactions on Microwave Theory and Techniques*, Vol. MTT-23, pp. 623-630, 1975.

13. A. Taflove, "Application of the Finite-Difference Time-Domain Method to Sinusoidal Steady-State Electromagnetic-Penetration Problems," *IEEE Transactions on Electromagnetic Compatibility*, Vol. EMC-22, pp. 191-202, 1980.
14. K. Umashankar and A. Taflove, "A Novel Method to Analyze Electromagnetic Scattering of Complex Objects," *IEEE Transactions on Electromagnetic Compatibility*, Vol. EMC-24, pp. 397-405, 1982.
15. R. Holland, "THREDE: A Free-Field EMP Coupling and Scattering Code," *IEEE Transactions on Nuclear Science*, Vol. NS-24, pp. 2416-2421, 1977.
16. K. S. Kunz and K. M. Lee, "A Three-Dimensional Finite-Difference Solution of the External Response of an Aircraft to a Complex Transient EM Environment. The Method and Its Implementation," *IEEE Transactions on Electromagnetic Compatibility*, Vol. 20, pp. 328-332, 1978.
17. J. Y. Chen, O. P. Gandhi, and D. L. Conover, "SAR and Induced Current Distributions for Operator Exposure to RF Dielectric Sealers," *IEEE Transactions on Electromagnetic Compatibility*, Vol. 33, pp. 252-261, 1991.
18. O. P. Gandhi, Y. G. Gu, J. Y. Chen, and H. I. Bassen, "SAR and Induced Current Distributions in a High-Resolution Anatomically Based Model of a Human for Plane-Wave Exposures 100-915 MHz," *Health Physics*, Vol. 63, pp. 281-290, 1992.
19. C. C. Johnson and A. W. Guy, "Nonionizing Electromagnetic Wave Effects in Biological Materials and Systems," *Proceedings of the IEEE*, Vol. 60, pp. 692-717, 1972.
20. M. A. Stuchly and S. S. Stuchly, "Dielectric Properties of Biological Substances - Tabulated," *Journal of Microwave Power*, Vol. 15, No. 1, pp. 19-26, 1980.
21. P. J. Dimbylow and O. P. Gandhi, "Finite-Difference Time-Domain Calculations of SAR in a Realistic Heterogeneous Model of the Head for Plane-Wave Exposure from 600 MHz to 3 GHz," *Physics in Medicine and Biology*, Vol. 36, pp. 1075-1089, 1991.
22. I. Chatterjee, O. P. Gandhi, M. J. Hagmann, and A. Riazi, "Plane-Wave Spectrum Approach for the Calculation of Electromagnetic Absorption Under Near-Field Exposure Conditions," *Bioelectromagnetics*, Vol. 1, pp. 363-377, 1980.
23. J. R. Mautz, "Mie Series Solution for a Sphere," *IEEE Transactions on Microwave Theory and Techniques*, Vol. MTT-26, p. 375, 1978.
24. T. W. Athey, M. A. Stuchly, and S. S. Stuchly, "Measurement of Radio Frequency Permittivity of Biological Tissues with an Open-Ended Coaxial Line: Part I," *IEEE Transactions on Microwave Theory and Techniques*, Vol. MTT-30, pp. 82-86, 1982.
25. M. A. Stuchly, T. W. Athey, G. M. Samaras, and G. E. Taylor, "Measurement of Radio Frequency Permittivity of Biological Tissues with an Open-Ended Coaxial Line: Part II - Experimental Results," *IEEE Transactions on Microwave Theory and Techniques*, Vol. MTT-30, pp. 87-92, 1982.

26. A. W. Guy, Personal communication (unpublished data).
27. G. Hartsgrove, A. Kraszewski, and A. Surowiec, "Simulated Biological Materials for Electromagnetic Radiation Absorption Studies," *Bioelectromagnetics*, Vol. 8, pp. 29-36, 1987.
28. A. R. Von Hippel, *Dielectric Materials and Applications*, John Wiley & Sons, New York, 1954.
29. H. I. Bassen and T. M. Babij, "Experimental Techniques and Instrumentation," Chapter 7 in *Biological Effects and Medical Applications of Electromagnetic Energy*, O. P. Gandhi, Editor, published by Prentice Hall, Englewood Cliffs, New Jersey, 07632, 1990.

LIST OF TABLES

1. Dielectric properties of the various tissues assumed for the model of the head and neck at 6 GHz.
2. Calculated absorbed powers and SARs for the three antennas for a radiated power of 0.6 W or 600 mW.
3. Compositions used to simulate the dielectric properties (ϵ_r , σ) of the soft tissues for the experimental model of the head.
4. Compositions used to simulate skull or bone at the experimental frequency of 6 GHz. Desired $\epsilon_r = 6.0$, $\sigma = 0.3$ S/m. The short-circuited waveguide method using different slab lengths [28] of the material was used for the measurements.
5. Calculated and measured values of maximum local SARs for Antennas 1 and 2. A radiated power of 600 mW is assumed for each of the antennas.

LIST OF FIGURES

1. A partial cross section of the millimeter-resolution model of the head passing through the upper part of the nose, the eyes, the nasal cavity, the ear, and the cerebellum. This is layer 45 of the model with layer no. 1 being the top layer of the body. Shown as the background is the grid of cell dimensions 1.974×1.974 m.
2. FDTD-calculated current distribution for a quarter-wave monopole antenna above ground versus theoretical cosine variation. Length of the monopole = $13 \delta = 12.5$ mm, $\delta = 0.9615$ mm, frequency = 6 GHz.
3. FDTD-calculated E-field variation for a lossy slab and its comparison with the analytical variation for plane waves. Also shown for comparison is the normalized E-field variation for the 2-element Yagi antenna. Note the faster decay for fields of limited transverse dimensions such as those for a Yagi antenna.
4. Electric-field distributions calculated for a 2/3 muscle-equivalent sphere of diameter 0.1 m for an irradiation frequency of 6 GHz. Shown for comparison are the analytical variations of fields obtained from Mie series solution [23]. Electrical properties taken for the sphere are: $\epsilon_r = 29.0$, $\sigma = 3.15$ S/m. A cell size $\delta = 2$ mm is taken for the calculations.
 - a. Magnitude of E_z versus y along the central y -axis.
 - b. Magnitude of E_y versus z along the central z -axis.
5. Geometrical arrangement for the centrally placed Antenna 1. The dimensions are shown in terms of the cell lengths δ_x , δ_y , and δ_z in the x -, y -, and z -directions, respectively. For the FDTD calculations, $\delta_x = \delta_y = 1.974$ mm, $\delta_z = 1.5$ mm.
6. Geometrical arrangement for Antenna 2. The dimensions are shown in terms of the cell lengths δ_x , δ_y , and δ_z in the x -, y -, and z -directions, respectively. For the FDTD calculations, $\delta_x = \delta_y = 1.974$ mm, $\delta_z = 1.5$ mm.
7. Geometrical arrangement for Antenna 3. This antenna is similar to Antenna 2 except that a somewhat wider and taller reflector is used. Also, the driven elements T and R (transmitting and receiving) are centrally located relative to their respective reflectors.
8. Layer-averaged SAR distributions for the high-resolution model of the head and neck.
 - a. Antenna 1 held against the right side of the head.
 - b. Antenna 2 held against the right and left sides of the head.
 - c. Antenna 3 held against the right and left sides of the head.

9. Calculated SAR distribution for three representative layers of the head for Antenna 2 held on the right side of the head. Layer no. 69 is in the xy plane containing the driving point of the antenna and layers 60 and 75 are 1.35 cm above and 0.9 cm below this plane, respectively. The axes x and y are from front to back, and from side to side of the head, respectively.
 - a. Layer no. 60.
 - b. Layer no. 69.
 - c. Layer no. 75.
10. Measured variations of the ϵ_r and σ for the various compositions of water, polyethylene powder and Superstuff at 6 GHz. No salt was used for any of the compositions while water content was varied to be 50, 60, 70, 80, and 90 percent. For the various water percentages the contents of polyethylene powder and Superstuff were (43,7), (33,7), (13,7), (23,7) and (6,4) percent, respectively.
 - a. Dielectric constant ϵ_r .
 - b. Conductivity σ .
11. Measured variation of conductivity σ for increasing salt (NaCl) content of the mixtures. For each of these mixtures the water and Superstuff contents were 70 and 7 percent, respectively. As the salt content was increased from 0.5 to 2.5 percent, the polyethylene powder content was reduced from 22.5 to 20.5 percent. Dielectric constant ϵ_r ($\approx 28-30$) did not vary much and hence is not shown.
12. Measured variation of conductivity σ for increasing salt (NaCl) content of the mixtures. For each of these mixtures the water and Superstuff contents were 70 and 7 percent, respectively. As the salt content was increased from 0.5 to 2.5 percent, the polyethylene powder content was reduced from 22.5 to 20.5 percent. Dielectric constant ϵ_r ($\approx 28-30$) did not vary much and hence is not shown.

Table 1. Dielectric properties* of the various tissues assumed for the model of the head and neck at 6 GHz.

Type [†]	Tissues	Dielectric constant ϵ_r	Conductivity σ (S/m)
0	air	1.0	0.0
1	muscle	40.0	4.9
2	fat	6.0	0.3
3	bone	6.0	0.3
4	cartilage	6.0	0.3
6	brain	30.0	5.3
11	blood	51.0	5.8
12	eye	30.0	3.8
17	CSF	72.0	6.7
18	vitreous humor	63.0	7.2
19	sclera/cornea	36.0	4.7
20	lens	30.0	3.8
29	ear**	23.0	2.6

* The assumed values for the various tissues are interpolated from the numbers given in references 19, 20 and 21.

† These numbers correspond to the tissue types used for the model of the whole body.

** Since the ear is composed of 50 percent cartilage, we have taken the electrical properties that are intermediate between those for muscle and cartilage.

Table 2. Calculated absorbed powers and SARs for the three antennas for a radiated power of 0.6 W or 600 mW.

Antenna	Side of the head	Total power absorbed by the head and neck mW	Whole-body-averaged SAR mW/kg	Spatial-peak SAR (1g) W/kg	Averaged SARs for some tissues (mW/kg)			
					<u>Brain</u>	<u>Humor</u>	<u>Lens</u> (for one eye)	<u>Sclera</u>
1	Right	4.4	0.06	0.25	0.32	0.74	1.65	2.64
2	Right	24.4	0.35	1.55	2.72	0.32	0.42	2.06
	Left	22.8	0.33	1.44	2.52	2.82*	5.75*	15.60*
3	Right	7.8	0.11	0.32	0.60	0.22	0.3	1.04
	Left	7.3	0.10	0.30	0.55	2.06*	4.04*	7.86*

* Because of the asymmetry of the antenna on the handset, the antenna is closer to the left eye when the handset is placed against the left ear. This results in somewhat larger SARs for the eye that is closer to the antenna. The SARs are, however, still fairly small and on the order of mW/kg.

Table 3. Compositions used to simulate the dielectric properties (ϵ_r , σ) of the soft tissues for the experimental model of the head.

Tissue	Desired		Test composition (percentage)				Measured	
	ϵ_r	σ S/m	H ₂ O	S.S.	P.E.P	NaCl	ϵ_r	σ S/m
brain	30.0	5.3	70.0	7.0	22.17	0.83	30.6	5.29
muscle	40.0	4.9	80.0	13.0	7.0	0	35.5	5.06
eyes	30.0	3.8*	92.0	3.2	3.0	1.8	46.0	6.8
vitreous humor	63.0	7.2						
ear	23.0	2.6	70.0	7.0	23.0	0	25.0	3.5

* Average of the properties desired for the eyes and the vitreous humor are used to develop the tissue-simulant material for this organ.

Table 4. Compositions used to simulate skull or bone at the experimental frequency of 6 GHz. Desired $\epsilon_r = 6.0$, $\sigma = 0.3$ S/m. The short-circuited waveguide method using different slab lengths [28] of the material was used for the measurements.

Mixture	<u>Test Composition (percentage)</u>			Slab length mm	<u>Measured</u>	
	Epoxy	KCl or NaCl Hardener	Solution*		ϵ_r	σ S/m
1	35.7	35.7	28.6 (KCl)	15.8	6.27	0.339
				22.0	5.78	0.32
2	35.7	35.7	28.6 (NaCl)	16.2	5.76	0.31

* The composition used for KCl or NaCl solution was 130 g of salt mixed with 950 g of water.

Table 5. Calculated and measured values of maximum local SARs for Antennas 1 and 2.
A radiated power of 600 mW is assumed for each of the antennas.

Antenna	Calculated W/kg	Measured W/kg
1	2.3	2.2
2	35.4	27.5

-
- * From the IEEE/ANSI safety guidelines [1] a volume averaging model for any 1 g of tissue (defined as a tissue volume in the shape of a cube). Spatial peak SARs for 1 g of tissue are, therefore, considerably lower and have been calculated as 0.25 and 1.55 W/kg for Antennas 1 and 2, respectively (see Table 2).

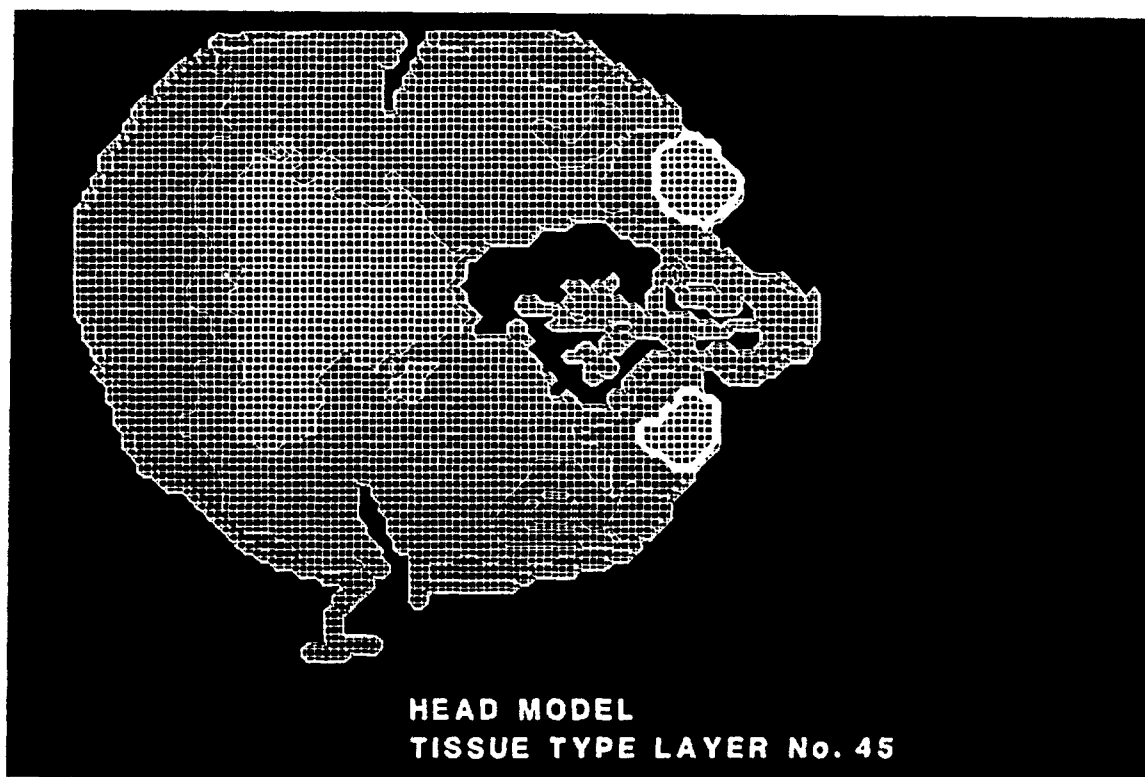


Fig. 1. A partial cross section of the millimeter-resolution model of the head passing through the upper part of the nose, the eyes, the nasal cavity, the ear, and the cerebellum. This is layer 45 of the model with layer no. 1 being the top layer of the body. Shown as the background is the grid of cell dimensions 1.974×1.974 mm.

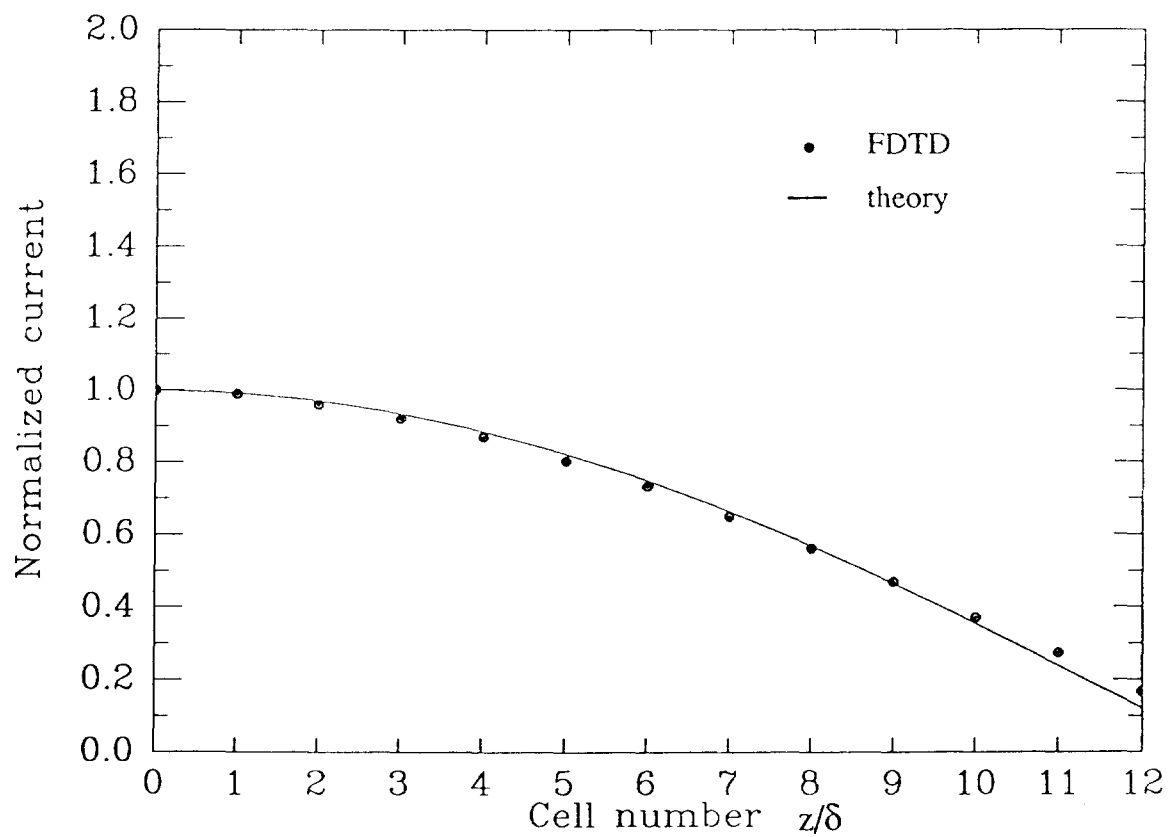


Fig. 2. FDTD-calculated current distribution for a quarter-wave monopole antenna above ground versus theoretical cosine variation. Length of the monopole = $13\delta = 12.5$ mm, $\delta = 0.9615$ mm, frequency = 6 GHz.

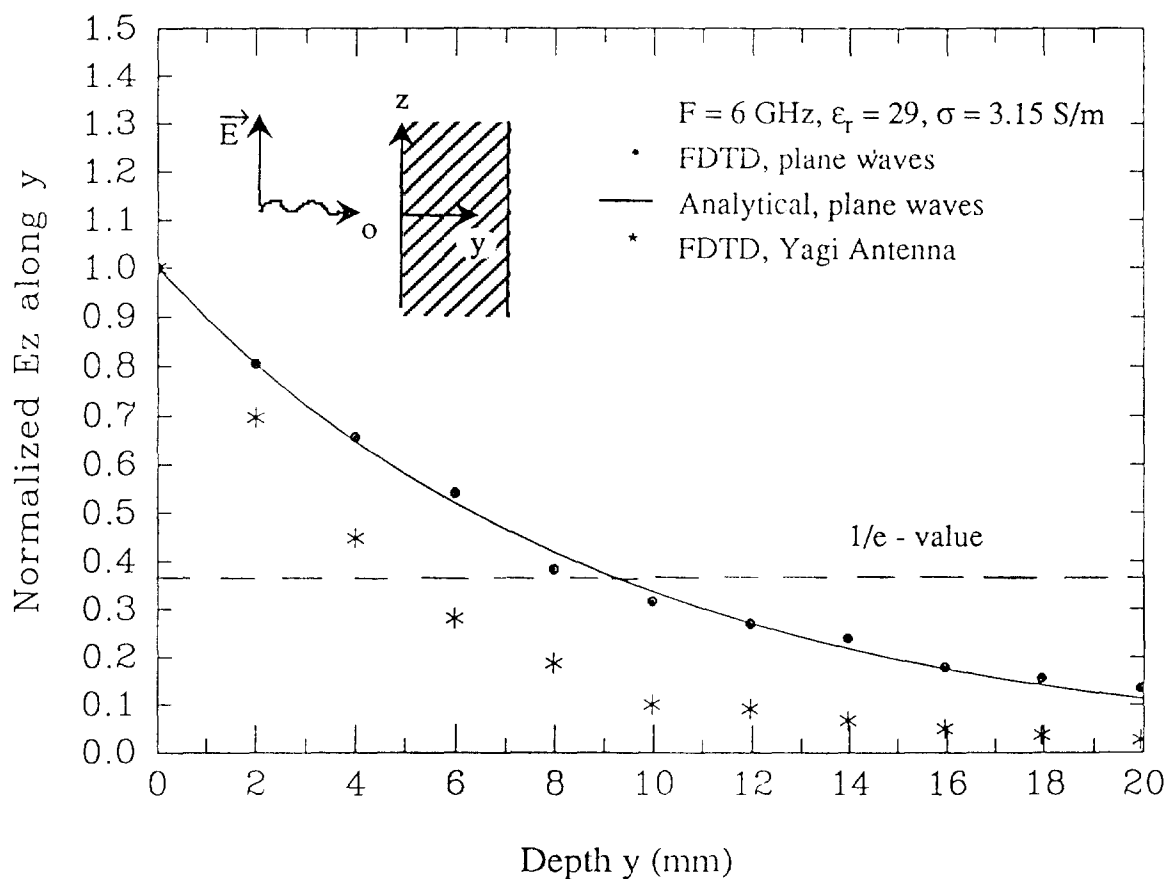
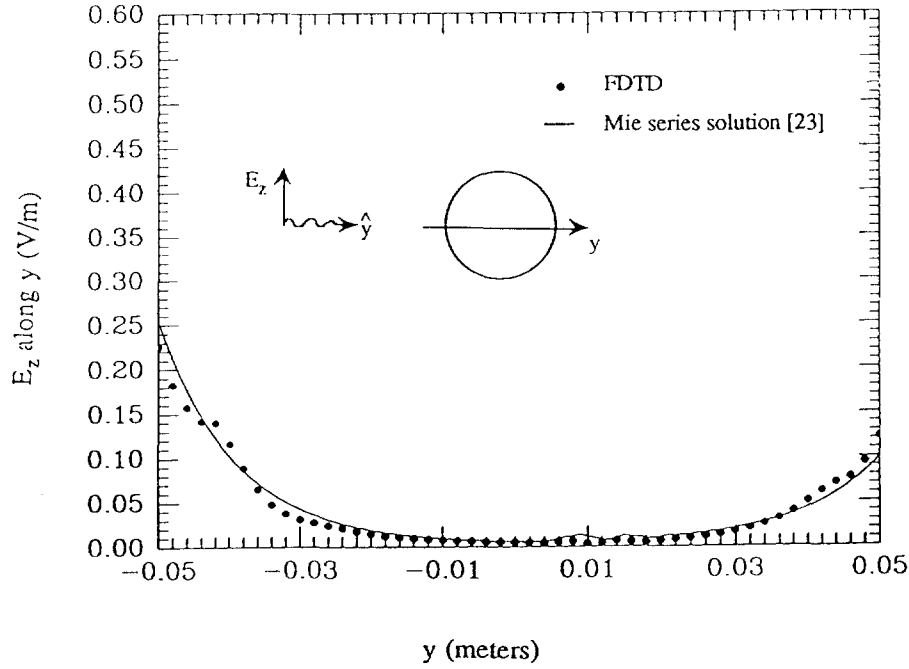


Fig. 3. FDTD-calculated E-field variation for a lossy slab and its comparison with the analytical variation for plane waves. Also shown for comparison is the normalized E-field variation for the 2-element Yagi antenna. Note the faster decay for fields of limited transverse dimensions such as those for a Yagi antenna.

a. Magnitude of E_z versus y along the central y-axis.



b. Magnitude of E_y versus z along the central z-axis.

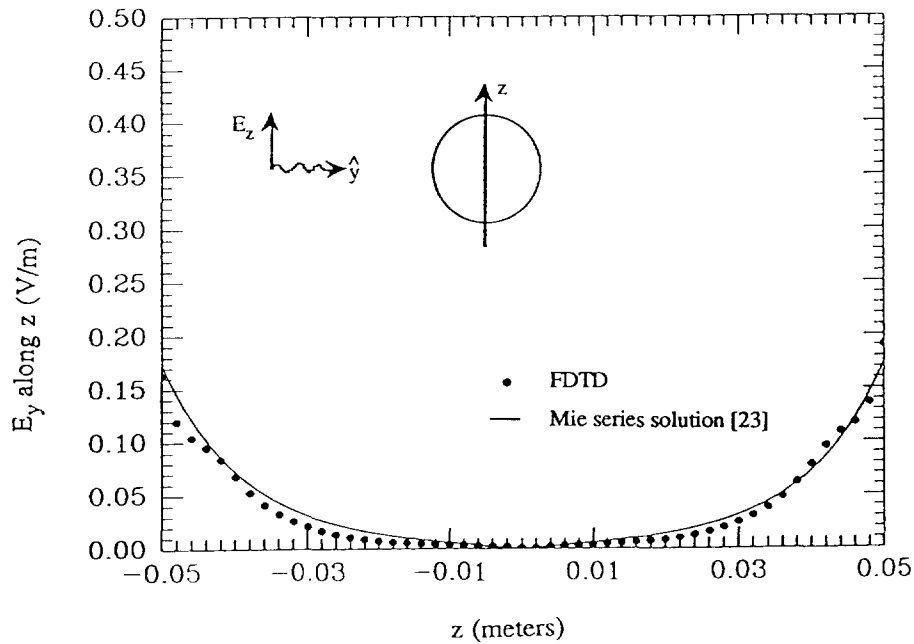


Fig. 4. Electric-field distributions calculated for a $2/3$ muscle-equivalent sphere of diameter 0.1 m for an irradiation frequency of 6 GHz. Shown for comparison are the analytical variations of fields obtained from Mie series solution [23]. Electrical properties taken for the sphere are: $\epsilon_r = 29.0$, $\sigma = 3.15$ S/m. A cell size $\delta = 2$ mm is taken for the calculations.

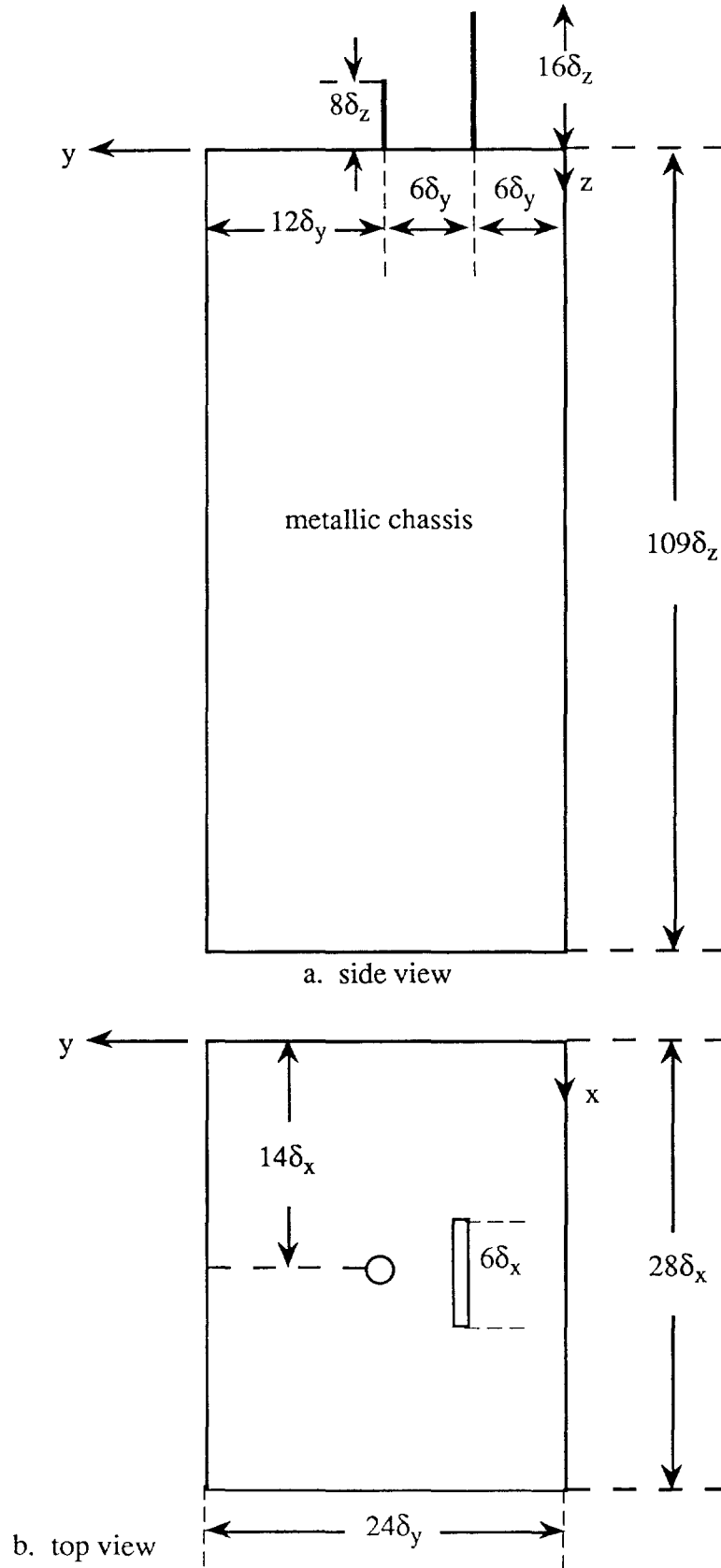


Fig. 5 Geometrical arrangement for the centrally placed **Antenna 1**. The dimensions are shown in terms of the cell lengths δ_x , δ_y , and δ_z in the x-, y-, and z-directions, respectively. For the FDTD calculations, $\delta_x = \delta_y = 1.974$ mm, $\delta_z = 1.5$ mm.